HEAD AND NECK

Perfusion imaging of parotid gland tumours: usefulness of arterial spin labeling for differentiating Warthin's tumours

Hiroki Kato[1] · Masayuki Kanematsu[1,2] · Haruo Watanabe[1] · Kimihiro Kajita[2] ·
Keisuke Mizuta[3] · Mitsuhiro Aoki[3] · Tomoyuki Okuaki[4]

Abstract

Objective To assess prospectively the efficacy of arterial spin labelling (ASL) against conventional and diffusion-weighted (DW) MR imaging for differentiating parotid gland tumours.

Methods We included 10 pleomorphic adenomas, 12 Warthin's tumours, and nine malignant tumours of the parotid glands. Only tumours larger than 10 mm were included in this study. All parotid gland tumours underwent T1-weighted, T2-weighted, DW, and ASL imaging. Tumour-to-parotid gland signal intensity ratios (SIRs) and apparent diffusion coefficients (ADCs) of solid components were correlated with these pathologies.

Results SIRs on T2-weighted images and ADCs were higher in pleomorphic adenomas than in Warthin's tumours ($p<.01$) and malignant tumours ($p<.01$). SIRs on ASL were higher in Warthin's tumours than in pleomorphic adenomas ($p<.01$) and malignant tumours ($p<.05$). Az value of SIRs on ASL for differentiating Warthin's tumours from the other pathologies was 0.982. The sensitivity, specificity, and accuracy of SIRs on ASL for the diagnosis of Warthin's tumours at an optimal SIR threshold of over 8.70 were 91.7 %, 94.7 %, and 93.5 %, respectively.

Conclusions ASL with SIR measurements could non-invasively evaluate tumour blood flow of parotid gland tumours and differentiate Warthin's tumours from pleomorphic adenomas and malignant tumours.

Key Points
- *ASL non-invasively evaluates tumour blood flow of parotid gland tumours*
- *ASL differentiates Warthin's tumours from pleomorphic adenomas and malignant tumours*
- *ASL cannot differentiate between pleomorphic adenomas and malignant tumours*

Keywords Arterial spin labelling · Diffusion-weighted imaging · Parotid gland · Salivary gland tumour · Warthin's tumour

✉ Hiroki Kato
hkato@gifu-u.ac.jp

[1] Department of Radiology, Gifu University School of Medicine, 1-1 Yanagido, Gifu 501-1194, Japan

[2] High-level Imaging Diagnosis Center, Gifu University Hospital, 1-1 Yanagido, Gifu 501-1194, Japan

[3] Department of Otolaryngology, Gifu University School of Medicine, Gifu, Japan

[4] Philips Healthcare, 2-13-37 Kohnan, Minato-ku, Tokyo 108-8507, Japan

Introduction

Salivary gland neoplasms account for approximately 3 % of all head and neck tumours. Fine needle aspiration cytology (FNAC) is the most used preoperative examination of salivary gland tumours due to their superficial nature and easy accessibility. A risk of FNAC is a possible spread of tumour cells, which can lead to a higher likelihood of local recurrence, especially in pleomorphic adenomas and malignant lesions [1]. Additionally, the differentiation of a few benign and malignant lesions might not only be difficult, but also impossible. Furthermore, a differentiation between a basal cell adenoma and a basal cell adenocarcinoma based solely on a FNAC is usually not possible [1].

Preoperative MR imaging has assumed a major role in surgical planning to assess the location and malignancy of these tumours. Conventional T1- and T2- weighted MR imaging have been used for the diagnosis of

salivary gland tumours; the infiltrative margin and hypointensity on T2-weighted images reportedly indicate malignancy [2, 3]. Furthermore, several authors have reported the usefulness of dynamic contrast-enhanced MR imaging, including the time–intensity curve (TIC), for the differentiation of salivary gland tumours [4–7]. The magnitude of peak enhancement is representative of the volume of the extravascular extracellular space, and the time to peak is representative of the extravascular extracellular space per contrast agent transfer to the tissue [8]. Recently, apparent diffusion coefficients (ADCs), calculated from diffusion-weighted (DW) MR imaging, have been evaluated as a possible biomarker. Because ADCs provide additional quantitative information related to random diffusion of water molecules in tissues, ADCs have also been reported to be useful in differentiating salivary gland tumours [9, 10]. However, ADCs alone did not allow differentiation between benign and malignant salivary gland tumours because low ADCs of Warthin's tumours can overlap with those of malignant tumours [9]. Therefore, the combination of dynamic contrast-enhanced and DW MR imaging could more accurately diagnose salivary gland tumours [11].

Arterial spin labelling (ASL) sequences for perfusion MR imaging have recently become available for use in clinical settings, offering a completely non-invasive technique for the quantitative evaluation of brain perfusion. This technique has proved reliable and reproducible in the assessment of cerebral blood flow (CBF) in various central nervous disorders, including cerebrovascular disease [12, 13], degenerative disease [14], and temporal lobe epilepsy [15]. Furthermore, this technique requires no extrinsic tracer, such as gadolinium chelates or radionuclides. It rather uses electromagnetically labelled arterial blood water as a freely diffusible intrinsic tracer. Therefore, it allows repetitive examination in patients with renal insufficiency and contrast media allergy. Subtraction of a control image without prior labelling produces perfusion-weighted images. Recently developed ASL imaging sequences, incorporating high-field, parallel imaging, pseudo-continuous labelling, and 3D imaging with background suppression, now provide a considerable increase in sensitivity for CBF in comparison with prior approaches [16].

Although some clinical studies using ASL have reported clinical utility in clarifying the differential diagnosis [17–21] and therapeutic efficacy [22] of brain tumours, the tumour blood flow (TBF) in patients with head and neck squamous cell carcinoma [23], and therapeutic response for nonsurgical treatment in head and neck cancer [24], we were unable to find any reports assessing the vascularity of salivary gland tumours using ASL. Therefore, this study aimed to assess the efficacy of ASL for the differentiation of parotid gland tumours in comparison with conventional and DW MR imaging.

Materials and methods

Patients

This study was approved by the human research committee of the institutional review board of our hospital and complied with the guidelines of the Health Insurance Portability and Accountability Act. Furthermore, written informed consent was provided by all study subjects at enrolment. Between July 2013 and September 2014, 44 consecutive patients with suspected parotid gland tumours underwent T1-weighted, T2-weighted, DW, and ASL imaging using a 3.0-T unit. However, five patients with histopathologically undiagnosed parotid gland tumours, three with small parotid gland tumours less than 10 mm in size, one with severe artefacts caused by dental metal, and three with histopathologically proven rare benign pathologies (one myoepithelioma, one oncocytoma, and one granulomatous lymphadenitis) were excluded from this study.

In total, 31 patients (age range, 34–84 years; mean 63 years; 17 men and 14 women) were included in the study. Among them, 10 patients had pleomorphic adenomas (age range, 34–72 years; mean 52 years; five men and five women), 12 had Warthin's tumours (age range, 42–79 years; mean 68 years; nine men and three women), and nine had malignant tumours (age range, 41–84 years; mean 69 years; three men and six women; three mucosa-associated lymphoid tissue lymphomas, two epithelial-myoepithelial carcinomas, one follicular lymphoma, one salivary duct carcinoma, one carcinoma ex pleomorphic adenoma, and one small cell carcinoma). Although five patients with Warthin's tumours and two with malignant lymphomas had multifocal or bilateral tumours, only the largest tumours were assessed. Thus, 31 parotid gland tumours of 31 patients were evaluated in this study.

The final diagnosis of parotid gland tumours was histopathologically performed by surgical resection in 20 patients or by fine needle aspiration biopsy in 11 patients. All patients underwent pathological examination within 1 month of their MR examination. The intervals between MR and pathological examination ranged from 1 to 30 days (mean, 12.4±7.1 days).

MR imaging

All 31 patients were examined using a 3-T MR imaging system (Achieva Quasar Dual 3 T; Philips Medical Systems, Best, Netherlands). A neurovascular array coil was used to allow coverage from the skull base to the thoracic inlet. Cardiac gating and respiratory triggering were not used, nor did we use an anti-susceptibility pad to reduce artefacts. All images were obtained in the transverse plane using the parallel imaging technique. Non-fat-suppressed T1-weighted spin-echo imaging (TR/TE, 778/15 ms; imaging matrices, 512×512; field of view, 20×20 cm; parallel imaging factor, 2.5; section thickness/gap, 4/1 mm), non-fat-suppressed T2-
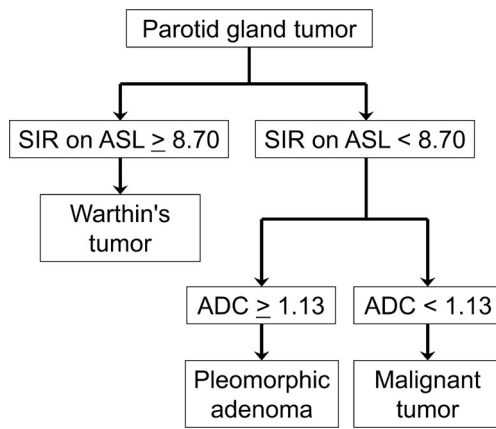
Fig. 1 Flow diagram combining SIRs on ASL and ADCs for the diagnosis of parotid gland tumours. When SIR on ASL is greater than 8.70, the lesion indicates Warthin's tumour. Among the tumours with SIR on ASL less than 8.70, when ADC is greater than 1.13 [$\times 10^{-3}$ mm^2/s], the lesion indicates pleomorphic adenomas. The remaining tumour indicates malignant tumour

weighted fast spin-echo imaging (TR/TE, 5,710/90 ms; imaging matrices, 512×512; field of view, 20×20 cm; parallel imaging factor, 2.3; section thickness/gap, 4/1 mm), and DW single-shot spin-echo echo-planar imaging (EPI) with fat suppression by using short-tau inversion recovery (STIR) (TR/TE/TI, 18,580/70/240 ms; imaging matrices, 256×256; field of view, 40×40 cm; parallel imaging factor, 2.0; section thickness/gap, 4/1 mm; b-value, 0 and 1,000 s/mm^2) were performed.

The perfusion imaging for the multi-phase signal targeting with alternating radio frequency ASL with the gradient echo type single-shot echo-planar imaging (MP-EPISTAR) were performed with following parameters (TR/TE , 250/15 ms; flip angle, 40°; imaging matrices, 80×80; field of view, 25×25 cm; parallel imaging factor, 2.3 ; echo-planar imaging factor, 37; section thickness/gap, 5/0.5 mm). There were eight slices per phase of MP-EPISTAR, and the centre of the eight slices was located in

the centre of the parotid gland tumours. The cycle duration of multi-phase was 4 s. The multi-phase acquisition was performed without a time interval between eight phases using Look-Locker readout of gradient echo EPI, with various delay times from 50 ms to 1,800 ms, with a constant interval of 250 ms. There were 30 acquisitions, resulting in a total acquisition time of 248 s. The label thickness was 13 cm and the position of the labelling plane was located 2 cm below the lowest imaging slices.

Image assessment

An experienced neuroradiologist (15 years of post-training experience of head and neck imaging), unaware of patient histories or pathology, reviewed all images. The reviewer measured the maximum diameter and signal intensity of parotid gland tumours by placing the largest possible regions of interest (ROIs) to encompass the solid components, while taking care to avoid cystic components and necrotic areas by referring to T2-weighted images. The reviewer also measured signal intensities of the contralateral normal parotid gland parenchyma at the same level as the tumours but excluded large vessels such as the retromandibular vein and the external carotid artery. Thus, the tumour-to-parotid gland signal intensity ratios (SIRs) of T1-weighted, T2-weighted, DW, and ASL imaging were calculated. SIRs on ASL were defined as the maximum SIRs in 8 phases of MP-EPISTAR. ADCs [$\times 10^{-3}$ mm^2/s] were also measured on ADC maps by placing ROIs over solid components of parotid gland tumours. For all ROI placements, the size, shape, and position of the ROIs were kept constant for all sequences by applying a copy-and-paste function at the workstation.

Statistical analyses

All statistical analyses were performed using SPSS version 18.0 (SPSS Inc, Chicago, IL, USA). The Welch test and

Table 1 Quantitative measurements of the parotid gland tumours

	Pleomorphic adenoma	Warthin's tumour	Malignant tumour
Maximum diameter (mm)	26.9±17.1	21.1±7.7	31.4±12.3
Tumour-to-parotid gland signal intensity ratios			
T1-weighted images	0.68±0.09	0.67±0.17	0.67±0.15
T2-weighted images	1.50±0.55*	0.65±0.13	0.80±0.22
Diffusion-weighted images	4.69±3.00	4.01±1.84	3.82±3.23
ASL	1.81±0.89	41.7±36.7**	5.09±5.27
ADC values ($\times 10^{-3}$ mm^2/s)	1.70±0.38*	0.78±0.18	0.88±0.32

Note – Data are shown as the mean±1 standard deviation

* The values of pleomorphic adenomas were significantly higher than those of Warthin's tumours ($p<.01$) and malignant tumours ($p<.01$)

** The values of Warthin's tumours were significantly higher than those of pleomorphic adenomas ($p<.01$) and malignant tumours ($p<.05$)

Tukey/Games–Howell post hoc test were used to compare the maximum diameters and SIRs between pleomorphic adenomas, Warthin's tumours, and malignant tumours. *P* values< 0.05 were considered significant. Receiver operating characteristic (ROC) curve analysis was used to determine the performance when differentiating Warthin's tumours from the other pathologies by SIRs on ASL. The sensitivity, specificity, and accuracy when diagnosing Warthin's tumours by SIRs on ASL were calculated. ROC curve analysis was also used to determine the ADC threshold when differentiating pleomorphic adenomas from the other pathologies by ADCs. The sensitivity, specificity, and accuracy when diagnosing Warthin's tumours, pleomorphic adenomas, and malignant tumours by using the combination of SIR threshold on ASL and ADC threshold were calculated. Figure 1 shows a flow diagram combining SIRs on ASL and ADCs for the diagnosis of parotid gland tumours.

Results

Quantitative measurements of maximum diameters and the SIRs of pleomorphic adenomas, Warthin's tumours, and malignant tumours are summarized in Table 1. *P* values between the parotid gland tumours are also shown in Table 2. No significant differences in maximum diameters were observed between pleomorphic adenomas (26.9 ± 17.1 mm) and Warthin's tumours (21.1 ± 7.7 mm; $p=0.539$), pleomorphic adenomas and malignant tumours (31.4 ± 12.3 mm; $p=0.718$), and Warthin's tumours and malignant tumours ($p=0.171$).

SIRs on T2-weighted images were higher in pleomorphic adenomas (1.50 ± 0.55) than in Warthin's tumours (0.65 ± 0.13; $p<.01$) and malignant tumours (0.80 ± 0.22; $p<.01$), but no significant difference was found between Warthin's tumours and malignant tumours ($p=0.188$). Similarly, ADCs were higher in pleomorphic adenomas ($1.70\pm0.38\times10^{-3}$ mm^2/s) than in Warthin's tumours ($0.78\pm0.18\times10^{-3}$ mm^2/s; $p<.01$)

and malignant tumours ($0.88\pm0.32\times10^{-3}$ mm^2/s; $p<.01$), but no significant difference was found between Warthin's tumours and malignant tumours ($p=0.701$) (Fig. 2a). On the other hand, SIRs on ASL were higher in Warthin's tumours (41.7 ± 36.7) than in pleomorphic adenomas (1.81 ± 0.89; $p<.01$) and malignant tumours (5.09 ± 5.27; $p<.05$), but no significant difference was found between pleomorphic adenomas and malignant tumours ($p=0.215$) (Figs. 2b, 3, 4 and 5). No significant differences in SIRs on T1-weighted images were observed between pleomorphic adenomas (0.68 ± 0.09) and Warthin's tumours (0.67 ± 0.17; $p=0.990$), pleomorphic adenomas and malignant tumours (0.67 ± 0.15; $p=0.979$), and Warthin's tumours and malignant tumours ($p=0.997$). Similarly, no significant differences in SIRs on DW images were observed between pleomorphic adenomas (4.69 ± 3.00) and Warthin's tumours (4.01 ± 1.84; $p=0.828$), pleomorphic adenomas and malignant tumours (3.82 ± 3.23; $p=0.762$), and Warthin's tumours and malignant tumours ($p=0.985$).

The AUC analysis to evaluate the diagnostic accuracy of SIRs on ASL for differentiating Warthin's tumours from the other two pathologies was 0.982. The sensitivity, specificity, and accuracy of SIRs on ASL for the diagnosis of Warthin's tumours at an optimal SIR threshold of over 8.70 were 91.7 %, 94.7 %, and 93.5 %, respectively.

The sensitivity, specificity, and accuracy using the combination of an optimal SIR threshold on ASL of 8.70 and an optimal ADC threshold of 1.13 [$\times10^{-3}$ mm^2/s] for the diagnosis of Warthin's tumours were 91.7 %, 94.7 %, and 93.5 %, respectively; those for the diagnosis of pleomorphic adenomas were 100.0 %, 90.5 %, and 93.5 %, respectively; and those for the diagnosis of malignant tumours were 55.6 %, 95.5 %, and 83.9 %, respectively.

Discussion

In our results, ASL could differentiate Warthin's tumours from the other two pathologies. Because malignant transformation

Table 2 *P* values between the parotid gland tumours

	Pleomorphic adenoma vs. Warthin's tumour	Pleomorphic adenoma vs. malignant tumour	Warthin's tumour vs. malignant tumour
Maximum diameter (mm)	0.539	0.718	0.171
Tumour-to-parotid gland signal intensity ratios			
T1-weighted images	0.990	0.979	0.997
T2-weighted images	0.002*	0.008*	0.188
Diffusion-weighted images	0.828	0.762	0.985
ASL	0.008*	0.215	0.014**
ADC values ($\times10^{-3}$ mm^2/s)	0.000*	0.000*	0.701

* *P* value was less than .01

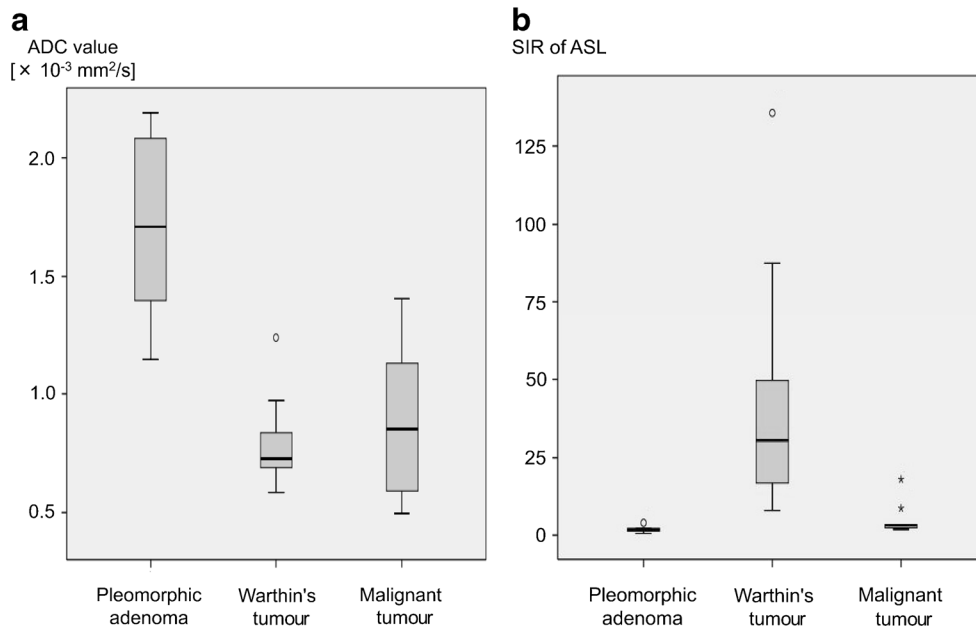** *P* value was less than .05

Fig. 2 Box and whisker plots showing quantitative measurements of ADCs and SIRs on ASL of three pathologies. *Boundary of boxes closest to zero* indicates 25th percentile, *line within boxes* indicates median, and *boundary of boxes farthest from zero* indicates 75th percentile. *Error bars* indicate smallest and largest values within 1.5 box lengths of 25th and 75th percentiles. Outliers are represented as *individual points*. **a**, ADCs were higher in pleomorphic adenomas ($1.70 \pm 0.38 \times 10^{-3}$ mm^2/s) than in Warthin's tumours ($0.78 \pm 0.18 \times 10^{-3}$ mm^2/s;

$p<.01$) and malignant tumours ($0.88 \pm 0.32 \times 10^{-3}$ mm^2/s; $p<.01$), but no significant difference was found between Warthin's tumours and malignant tumours ($p=0.701$). **b**, SIRs on ASL were higher in Warthin's tumours (41.7 ± 36.7) than in pleomorphic adenomas (1.81 ± 0.89; $p<.01$) and malignant tumours (5.09 ± 5.27; $p<.05$), but there was no significant difference in SIRs on ASL between pleomorphic adenomas and malignant tumours ($p=0.215$)

is extremely rare, occurring in only 0.3 % of all Warthin's tumours [25], a limited partial parotidectomy is the recommended treatment for Warthin's tumour. If the preoperative diagnosis of Warthin's tumours is reliable, conservative observation is also a reasonable management option. In contrast, malignant transformation of pleomorphic adenomas is not rare, with the incidence of malignancy being correlated with their duration. In addition, pleomorphic adenomas appear as round masses with protrusions into surrounding tissue. If pleomorphic adenomas are treated by enucleation, the protrusions

remain. Because of the risk of recurrence and malignant transformation, radical surgical excision is required for pleomorphic adenomas as with malignant salivary gland tumours. Therefore, the ability to differentiate Warthin's tumours from these pathologies is important when deciding the appropriate treatment strategy in parotid gland tumours.

Dynamic contrast-enhanced MR imaging using TIC assessments is useful in differentiating salivary gland tumours [4–7]. In most pleomorphic adenomas, TIC shows a continuously and gradually increased enhancement, and the time of
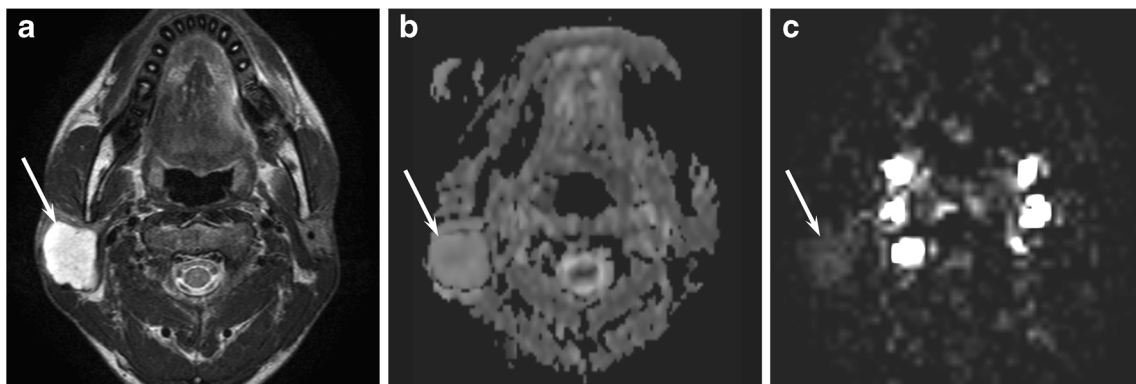

Fig. 3 A 34-year-old man with a pleomorphic adenoma of the right parotid gland. **a**, T2-weighted fast spin-echo MR image (TR/TE, 5,710/90 ms) shows a lobulated, well-demarcated, and markedly hyperintense lesion (*arrow*) in the right parotid gland. **b**, ADC map shows high ADC value (2.09×10^{-3} mm^2/s) (*arrow*). **c**, ASL image shows low SIR value (1.67) (*arrow*)
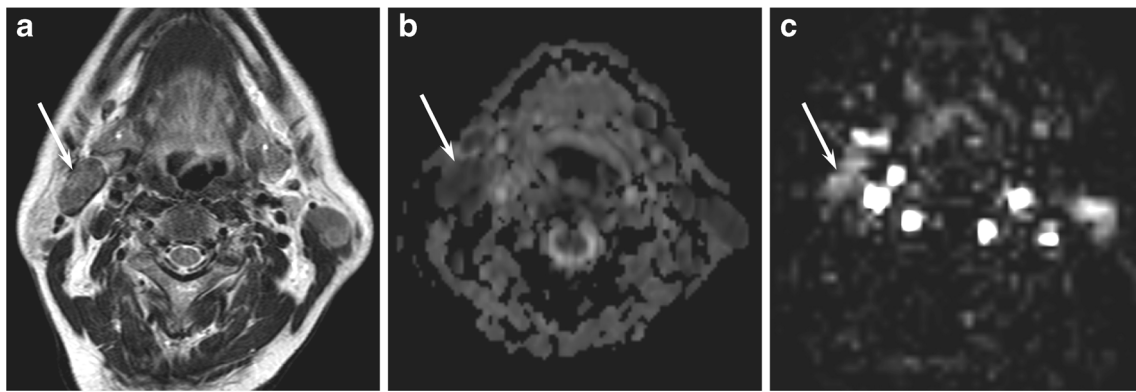
Fig. 4 A 62-year-old man with Warthin's tumours of the bilateral parotid glands. **a**, T2-weighted fast spin-echo MR image (TR/TE, 5,710/90 ms) shows the largest lesion (*arrow*) with well-demarcated margin and hypointensity in lower pole of the right parotid glands. **b**, ADC map shows low ADC value (0.70×10^{-3} mm^2/s) in the right parotid gland lesion (*arrow*). **c**, ASL image shows high SIR value (87.45) in the right parotid gland lesion (*arrow*)

peak enhancement is typically longer than 120 s [4–7]. Histopathologically, pleomorphic adenomas comprise the mesenchymal-like components of mucoid/myxoid, cartilaginous, or hyalinized materials as products of myoepithelial cells. The tumour areas with myxomatous or fibrous connective tissues have tended to exhibit gradual enhancement with a prolonged time of peak enhancement [5]. In some pleomorphic adenomas, the time of peak enhancement is shorter than 120 s and weak washout is observed due to the hypercellularity of epithelial components [4, 5]. In any case, because pleomorphic adenomas are hypovascular tumours, SIRs on ASL in pleomorphic adenomas were lowest among three pathologies in our series.

In Warthin's tumours, TIC generally shows rapid enhancement with high washout. The time of peak enhancement is definitely shorter than 120 s [4–6], typically shorter than 60 s [7]. The washout ratios determined from the TIC of Warthin's tumours are generally greater than 30 % [4, 5, 7]. Histopathologically, Warthin's tumours comprise varying proportions of oncocytic epithelium and lymphoid stroma. The

dense lymphoid stroma often looks similar to a normal lymph node, complete with lymphoid follicles and germinal centres. The tumour areas of hypercellularity, such as the densely packed lymphoid tissue of Warthin's tumours, exhibit rapid enhancement with high washout [5]. As with these published data on TIC assessments, SIRs on ASL in Warthin's tumours were significantly greatest in our series due to the hypervascular nature.

Because malignant salivary gland tumours include various histological subtypes and grades, malignant salivary gland tumours do not have uniform imaging findings. The TIC of adenoid cystic carcinomas show a similar pattern to pleomorphic adenomas, because adenoid cystic carcinomas also have an increased interstitial space with extracellular mucin [6]. On the other hand, the TIC of acinic cell carcinomas show rapid enhancement with high washout similarly to Warthin's tumours because of their high cellularity [11]. However, in most malignant salivary gland tumours, the time of peak enhancement is shorter than 120 s and the washout ratios are less than 30 % [4–7]. In our series, SIRs on ASL in malignant salivary
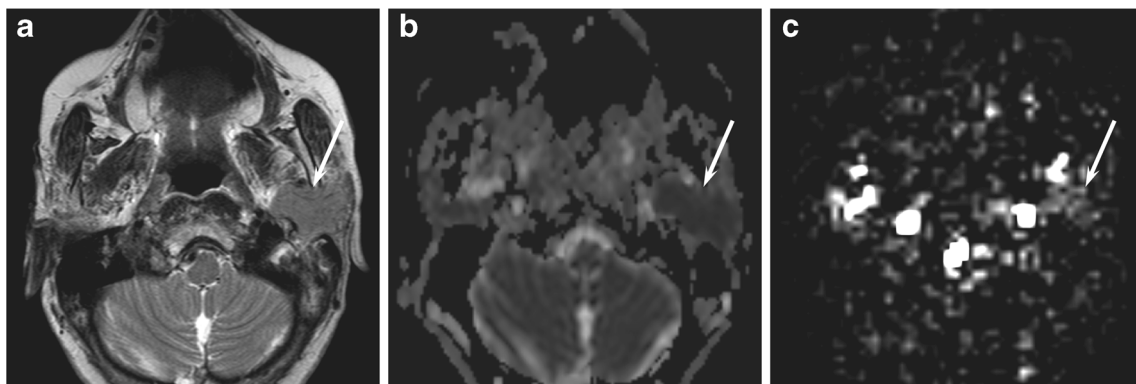

Fig. 5 A 77-year-old man with a mucosa-associated lymphoid tissue lymphoma of the left parotid gland. **a**, T2-weighted fast spin-echo MR image (TR/TE, 5,710/90 ms) shows a partially ill-demarcated, isointense lesion (*arrow*) in the left parotid gland. **b**, ADC map shows extremely low ADC value (0.59×10^{-3} mm^2/s) (*arrow*). **c**, ASL image shows low SIR value (3.17) (*arrow*)

gland tumours ranged in values, and SIRs on ASL in some malignant tumours overlapped with those of Warthin's tumours. However, mean SIRs on ASL in malignant tumours were significantly lower than those of Warthin's tumours.

Recently, the usefulness of DW imaging with ADC measurement has been reported using a 3-T MR unit [26]. As with our results, they reported that mean ADCs of Warthin's tumours were significantly lower than those of pleomorphic adenomas [26]. However, they could not differentiate between benign and malignant tumours due to the overlap of ADCs between Warthin's tumours and malignant tumours [26]. Our results also showed no significant differences of ADCs between Warthin's tumours and malignant tumours. This is a clinical dilemma because Warthin's tumours require the less aggressive surgical approach, whereas malignant tumours require superficial or total parotidectomy with or without facial nerve resection. The main aspect and gain of our study is the differentiation potential of ASL between Warthin's tumours and malignant tumours.

ASL technique has been successfully used to evaluate various central nervous disorders, including cerebrovascular disease, degenerative disease, and temporal lobe epilepsy, but ASL recently has applied for the head and neck region [23, 24]. ASL has been reported to be a useful tool for non-invasive assessments of the TBF in patients with head and neck squamous cell carcinoma [23] and those of therapeutic response for nonsurgical treatment in head and neck cancer [24].

The present study has several limitations. First, because the study was conducted at a single institution, the cohort was small. The number of malignant tumours is especially small. Thus, we propose that a multi-centre study be conducted to clarify the clinical impact across a larger and more representative cohort. Second, we could not measure the perfusion parameters of TBF and time to peak (TTP) because we did not obtain the true signal data as an equilibrium magnetization. If we calculated this signal data from signal intensity of blood-filled voxel in internal carotid vein at the last phase, the calculated signal data would be lower than true signal data because we used Look-Locker method. Third, because dynamic contrast-enhanced MR imaging was not performed, we could not compare its diagnostic accuracy against ASL, which will require further investigation.

In conclusion, SIRs on ASL were significantly higher for Warthin's tumours when compared to both pleomorphic adenomas and malignant tumours. However, there was no significant difference in SIRs on ASL between pleomorphic adenomas and malignant tumours. Although it has been difficult to differentiate between Warthin's tumours and malignant tumours by using DW imaging with ADC measurement, we demonstrated the high diagnostic accuracy of ASL for differentiating Warthin's tumours from malignant tumours, which we assumed to be due to the hypervascular nature of Warthin's

tumours. Our results also suggest that the combination of ASL and DW imaging offers a high potential for differentiating the three most important groups of parotid gland tumours (pleomorphic adenomas, Warthin's tumours, and malignant tumours) non-invasively.

References

1. Das DK, Petkar MA, Al-Mane NM, Sheikh ZA, Mallik MK, Anim JT (2004) Role of fine needle aspiration cytology in the diagnosis of swellings in the salivary gland regions: a study of 712 cases. Med Princ Pract 13:95–106
2. Som PM, Biller HF (1989) High-grade malignancies of the parotid gland: identification with MR imaging. Radiology 173:823–826
3. Christe A, Waldherr C, Hallett R, Zbaeren P, Thoeny H (2011) MR imaging of parotid tumors: typical lesion characteristics in MR imaging improve discrimination between benign and malignant disease. AJNR Am J Neuroradiol 32:1202–1207
4. Yabuuchi H, Fukuya T, Tajima T, Hachitanda Y, Tomita K, Koga M (2003) Salivary gland tumors: diagnostic value of gadolinium-enhanced dynamic MR imaging with histopathologic correlation. Radiology 226:345–354
5. Eida S, Ohki M, Sumi M, Yamada T, Nakamura T (2008) MR factor analysis: improved technology for the assessment of 2D dynamic structures of benign and malignant salivary gland tumors. J Magn Reson Imaging 27:1256–1262
6. Tsushima Y, Matsumoto M, Endo K (1994) Parotid and parapharyngeal tumours: tissue characterization with dynamic magnetic resonance imaging. Br J Radiol 67:342–345
7. Hisatomi M, Asaumi J, Yanagi Y et al (2007) Diagnostic value of dynamic contrast-enhanced MRI in the salivary gland tumors. Oral Oncol 43:940–947
8. Muller-Schimpfle M, Noack F, Oettling G et al (2000) Influence of histopathological factors on dynamic MR mammography. Röfo 172:894–900
9. Matsushima N, Maeda M, Takamura M, Takeda K (2007) Apparent diffusion coefficients of benign and malignant salivary gland tumors. Comparison to histopathological findings. J Neuroradiol 34:183–189
10. Habermann CR, Arndt C, Graessner J et al (2009) Diffusion-weighted echo-planar MR imaging of primary parotid gland tumors: is a prediction of different histologic subtypes possible? AJNR Am J Neuroradiol 30:591–596
11. Yabuuchi H, Matsuo Y, Kamitani T et al (2008) Parotid gland tumors: can addition of diffusion-weighted MR imaging to dynamic contrast-enhanced MR imaging improve diagnostic accuracy in characterization? Radiology 249:909–916
12. Detre JA, Alsop DC, Vives LR, Maccotta L, Teener JW, Raps EC (1998) Noninvasive MRI evaluation of cerebral blood flow in cerebrovascular disease. Neurology 50:633–641

13. Chalela JA, Alsop DC, Gonzalez-Atavales JB, Maldjian JA, Kasner SE, Detre JA (2000) Magnetic resonance perfusion imaging in acute ischemic stroke using continuous arterial spin labeling. Stroke 31:680–687

14. Alsop DC, Detre JA, Grossman M (2000) Assessment of cerebral blood flow in Alzheimer's disease by spin-labeled magnetic resonance imaging. Ann Neurol 47:93–100

15. Wolf RL, Alsop DC, Levy-Reis I et al (2001) Detection of mesial temporal lobe hypoperfusion in patients with temporal lobe epilepsy by use of arterial spin labeled perfusion MR imaging. AJNR Am J Neuroradiol 22:1334–1341

16. Wolf RL, Detre JA (2007) Clinical neuroimaging using arterial spin-labeled perfusion magnetic resonance imaging. Neurotherapeutics 4:346–359

17. Warmuth C, Gunther M, Zimmer C (2003) Quantification of blood flow in brain tumors: comparison of arterial spin labeling and dynamic susceptibility-weighted contrast-enhanced MR imaging. Radiology 228:523–532

18. Wolf RL, Wang J, Wang S et al (2005) Grading of CNS neoplasms using continuous arterial spin labeled perfusion MR imaging at 3 Tesla. J Magn Reson Imaging 22:475–482

19. Kimura H, Takeuchi H, Koshimoto Y et al (2006) Perfusion imaging of meningioma by using continuous arterial spin-labeling: comparison with dynamic susceptibility-weighted contrast-enhanced MR images and histopathologic features. AJNR Am J Neuroradiol 27:85–93

20. Noguchi T, Yoshiura T, Hiwatashi A et al (2008) Perfusion imaging of brain tumors using arterial spin-labeling: correlation with histopathologic vascular density. AJNR Am J Neuroradiol 29:688–693

21. Jarnum H, Steffensen EG, Knutsson L et al (2010) Perfusion MRI of brain tumours: a comparative study of pseudo-continuous arterial spin labelling and dynamic susceptibility contrast imaging. Neuroradiology 52:307–317

22. Weber MA, Thilmann C, Lichy MP et al (2004) Assessment of irradiated brain metastases by means of arterial spin-labeling and dynamic susceptibility-weighted contrast-enhanced perfusion MRI: initial results. Investig Radiol 39:277–287

23. Fujima N, Kudo K, Tsukahara A et al (2014) Measurement of tumor blood flow in head and neck squamous cell carcinoma by pseudo-continuous arterial spin labeling: comparison with dynamic contrast-enhanced MRI. J Magn Reson Imaging. doi:10.1002/jmri.24637

24. Fujima N, Kudo K, Yoshida D et al (2014) Arterial spin labeling to determine tumor viability in head and neck cancer before and after treatment. J Magn Reson Imaging 40:920–928

25. Batsakis JG (1987) Carcinoma ex papillary cystadenoma lymphomatosum. Malignant Warthin's tumor. Ann Otol Rhinol Laryngol 96:234–235

26. Fruehwald-Pallamar J, Czerny C, Holzer-Fruehwald L et al (2013) Texture-based and diffusion-weighted discrimination of parotid gland lesions on MR images at 3.0 Tesla. NMR Biomed 26:1372–1379